Available online at www.sciencedirect.com

ScienceDirect

Proceedings of the Combustion Institute 36 (2017) 1259–1267

Proceedings of the Combustion Institute

www.elsevier.com/locate/proci

Experimental and kinetic modeling study of laminar coflow diffusion methane flames doped with *iso*-butanol

Hanfeng Jin [a], Guoqing Wang [a], Yizun Wang [a], Xiaoyuan Zhang [a], Yuyang Li [b,*], Zhongyue Zhou [b], Jiuzhong Yang [a], Fei Qi [a,b]

[a] *National Synchrotron Radiation Laboratory, University of Science and Technology of China, Hefei, Anhui 230029, PR China*

[b] *Key Laboratory for Power Machinery and Engineering of MOE, Shanghai Jiao Tong University, Shanghai 200240, PR China*

Received 4 December 2015; accepted 15 June 2016
Available online 25 June 2016

Abstract

In this work, laminar coflow diffusion flames fueled with methane/*iso*-butanol were investigated with synchrotron vacuum ultraviolet photoionization mass spectrometry (SVUV-PIMS). Mole fractions of C_2–C_{16} flame species, including small hydrocarbons, oxygenates and aromatics were measured along the flame centerline. The enhancement in the formation of aromatics was observed through the increment of the *iso*-butanol doping ratio (1.95% and 3.90% in two flames) in the inlet fuel gas mixture. A detailed kinetic model was developed from previous models to help understand the experimental findings. According to rate of production analysis in laminar coflow diffusion flames, unimolecular decomposition and H abstraction reactions provide equivalent contributions to the consumption of *iso*-butanol. Compared to the coflow flames doped with other butanol isomers with the identical condition, the water elimination reaction of *iso*-butanol has the lowest contribution to fuel consumption. Two reaction pathways provide major contribution to the formation of propargyl radical, i.e. $iC_4H_9OH \rightarrow iC_3H_7 \rightarrow C_3H_6 \rightarrow aC_3H_5 \rightarrow aC_3H_4 \rightarrow C_3H_3$ and $iC_4H_9OH \rightarrow \beta C_4H_8OH \rightarrow iC_4H_8 \rightarrow iC_4H_7 \rightarrow aC_3H_4 \rightarrow C_3H_3$. Propargyl is concluded as the key precursor for aromatics, while phenyl and benzyl radicals are the main PAH precursors. Finally, based on the studies of laminar coflow flames fueled with butanol isomers, the sooting tendency of butanol isomers relates strictly to the efficiency of the propargyl formation pathways in fuel decomposition.

Keywords: Laminar coflow diffusion flame; *Iso*-butanol; SVUV-PIMS; Kinetic modeling; Formation of benzene and PAHs

1. Introduction

The interest in accessible and environmentally friendly transportation fuels has raised up due to an increased awareness of the harmful emissions

* Corresponding author.
E-mail addresses: yuygli@sjtu.edu.cn, yuygli@ustc.edu.cn (Y. Li), fqi@sjtu.edu.cn (F. Qi).

http://dx.doi.org/10.1016/j.proci.2016.06.111
1540-7489

associated with the burning of fossil fuels. Biobutanol is a promising alternative for conventional fuel because of its advantages compared to bioethanol, such as higher energy density, better miscibility with practical fuels, and lower water affinity. *Iso*-butanol (iC$_4$H$_9$OH), in particular, has attracted attentions as a viable isomer for commercialization [1].

A series of experimental studies [2] have been performed in order to improve the understanding of the combustion chemistry of *iso*-butanol. Yasunaga et al. [3] and Cai et al. [4] measured the concentrations of its pyrolysis species, respectively. Stranic et al. [5] focused on the time history of particular species in its pyrolysis, such as OH radical, etc. Togbé et al. [6] investigated its oxidation in a jet-stirred reactor at 10 atm, while Yang et al. [7], Oßwald et al. [8] and Hansen et al. [9] studied its oxidation process in premixed flat flames at 30 torr. On the PAH formation tendency of *iso*-butanol, McEnally et al. [10] and Jin et al. [11] performed individual experiments with different diagnostic methods but achieved similar conclusion: *iso*-butanol has a medium tendency which is lower than *tert*-butanol but higher than *n*- and *sec*-butanol. Besides, the measurements of laminar flame speed [12–15] and ignition delay time [3,16,17] at various pressures and equivalence ratios were also carried out. Based on these available experimental data, several kinetic models have been proposed recently [3,4,17–19].

McEnally and Pfefferle [10,20] studied the sooting tendencies of a series of hydrocarbons and oxygenates, which revealed that the value of butanol was lower than *n*-heptane (the gasoline model fuel), but was comparable with butane. Considering the potential of *iso*-butanol as a substitute in internal engines [21,22], it is urgently desired to better understand the PAH formation mechanism in the combustion of *iso*-butanol. Therefore, laminar coflow diffusion methane/*iso*-butanol flames were studied using synchrotron vacuum ultraviolet photoionization mass spectrometry (SVUV-PIMS) at atmospheric pressure in this work. A model including PAH formation sub-mechanism was developed based on previous *iso*-butanol [4] and methane [23] models. It was validated by both the new laminar coflow diffusion flame dada and the experimental data reported in literatures [4–6,12,13,18]. With the help of rate of production (ROP) analysis, important intermediates and key reactions were characterized in the decomposition of *iso*-butanol and the formation of PAHs, which were compared to our previous studies on other butanol isomers [24–26].

2. Experimental methods

The laminar coflow diffusion flame experiment was performed at National Synchrotron Radiation Laboratory in Hefei, China. The coflow flame apparatus was introduced in detail in previous studies [11], only a brief description will be given here. The coflow flame burner consisted of a 10-mm-ID stainless steel fuel tube nested in the center of a 102-mm-ID co-flow air tube. It was fixed on a two dimensional translational stage that can be moved with high precision (<0.05 mm) towards the specific sampling position. Flame species along the centerline of coflow flame were sampled by a quartz probe. The flame conditions are listed in Table 1. The purities of samples, including CH_4, N_2, Ar and iC$_4$H$_9$OH are 99.995%, 99.999%, 99.99% and 99%, respectively. The gas flow rates were regulated by mass flow controllers, and the liquid *iso*-butanol was injected into a vaporizer with a chromatography pump. In order to avoid the condensation of *iso*-butanol, the temperatures of the vaporizer and the gas mixture transferring in pipes were kept at 410 and 493 K, respectively. The inlet mole fractions of the fuel mixture, including the fuels (CH_4 and iC$_4$H$_9$OH), the diluent gas (N_2), and the calibration gas (Ar), varied in two different flame conditions, while the carbon flux was kept identical. The mean velocities of fuel mixture and air under standard condition were 13.33 and 16.48 cm/s in both flames, respectively. The uncertainty of SVUV-PIMS measurements is related to the sampling process and the photoionization cross sections (PICS) of flame species. Generally, it is within ± 10% for flame species calculated with cold gas calibration, ± 25% for stable flame species with known PICSs, and about a factor of 2 for free radicals and the flame species with estimated PICSs [11]. The PICSs of flame species are available in the online database [27].

Table 1
Experimental conditions of coflow flames[(a)].

Name	Q_{air}	Q_{Ar}	Q_{N_2}	Q_{CH_4}	$Q_{iC_4H_9OH}$
CF1	80,000	5.87	438	160	24.50
CF2	80,000	5.87	401	209	12.25

[(a)] Q_i, flow rate of species i, Unit: SCCM. The liquid flow rate of iso-butanol is converted into its gas flow rate in standard condition.

3. Kinetic model construction and numerical simulation

The kinetic model in this work was developed from our previous *iso*-butanol [4] and methane [23] models. The sub-mechanism of *iso*-butanol was slightly modified from the model of Cai et al. [4], while the sub-mechanism of *iso*-butene was upgraded according to our recent modeling work of *tert*-butanol (see *Supplemental materials*) [24]. The unimolecular decomposition reactions of iso-butanol were referred to the calculation of

Zhou et al. [28]. Since the C–O bond dissociation of *iso*-butanol is not important according to the theoretical and modeling studies [28], and provides negligible contributions in pyrolysis, premixed and counterflow diffusion flames [4,19], it is not included in this model for coflow diffusion flame. The optimized rate constants of Stranic et al. [5] on the H abstraction reactions of *iso*-butanol by H atom were adopted in this model, while the rate constants of H abstraction reactions by OH radical were refitted based on the theoretical and experimental results of Zheng et al. [29] and Pang et al. [30]. The PAH formation sub-mechanism in this model was mainly taken from the previous models [23,31–34]. The thermodynamic and transport properties were taken from [4,23,35,36] or estimated following the procedure in [37]. Besides the validation on the new coflow diffusion flame data, comprehensive validations of this model were performed on the experimental data from literatures [4–6,12,13,18]. All of the external validation results and the kinetic model files in CHEMKIN format are provided in *Supplemental materials*.

Numerical simulation of coflow flames was performed with laminarSMOKE [38], which was introduced in former studies [23,26]. Both Fickian diffusion and Soret effect [39] were taken into account in the simulation, as well as the radiation heat transfer [40]. A stretched, two-dimensional, rectangular control domain, with a length of 297 mm and a width of 58 mm was adopted in simulation, because of the axial symmetry of coflow flames. A fine numerical grid with uniform cell spacing was built for the flame region, while a coarse grid was used in the outer area. A grid with 9504 cells (144 in flame height and 66 in radial direction) was fine enough in order to balance the accuracy of the calculation and the cost of computational time [23]. The inlet flow conditions followed the values in Table 1.

4. Results and discussions

More than 40 species were observed in laminar coflow diffusion flames. The model predictions of these species were presented in Figs. 1–4. Considering the uncertainties in the experimental and modeling results, a good agreement between them can be observed, which is consistent with the good performance of this model in predicting the experimental data of pyrolysis, oxidation, premixed flames and counterflow diffusion flames of *iso*-butanol in literatures (as shown in the *Supplemental materials*). The 1.95% deviation of *iso*-butanol in the inlet mole fraction with identical carbon flux could rarely impact the major products, however, result in a significant influence on the C_3–C_4 intermediates and the participants in subsequent carbon chain growth process.

As discussed in previous studies [23,25], the coflow diffusion flame is driven by two major effects, the mass diffusion and the chemical reaction. In the flame region where the gas temperature is beyond 1000 K (over 20 mm above burner surface along the flame centerline, as shown in Fig. 1), chemical reactions are considered active enough to control the behavior of coflow flame. Whilst in low temperature region, diffusion effect strongly impacts the spatial distribution of flame species. The fuel diffuses radially towards the flame front, and the hydrocarbon products formed in the region close to the flame front diffuse in the opposite direction. Therefore, local ROP analysis was performed along the centerline to illustrate the effect of chemical reaction, and these values were then integrated with the height above burner surface until the tip of flame, named as global ROP. Generally, both of them reveal the same conclusions [23,24]. Since the reaction pathways in CF1 and CF2 are very similar, the following discussion will take CF1 as an example.

4.1. Decomposition of iso-butanol

According to the global ROP analysis in Fig. 5, the decomposition procedure of *iso*-butanol in the center area of coflow diffusion flame is very similar to that under pyrolysis condition [4]. Coflow flame is enveloped by its flame front, thus the mass transfer of oxygen molecule or oxygenated radicals cannot easily reach the center of the flame. Therefore, it is a proximate pyrolysis environment, and its reaction network is controlled by locally produced active intermediates [23]. As a result, unimolecular decomposition and H abstraction reactions provide equivalent contributions in the consumption of *iso*-butanol. Obviously, the C–C bond dissociation yielding iC_3H_7 and CH_2OH radicals (R1) is the most efficient one, which consumes 30% of the fuel. Other unimolecular decomposition reactions of *iso*-butanol, like the unimolecular water elimination reaction (R2) and the C–C bond dissociation producing $CH_3CH^*CH_2OH$ radical (R3), provide additional contributions of 7% and 10%. The contribution of water elimination reaction in *iso*-butanol doped flame is relatively low compared to the situation in flames of other butanol isomers (16%, 45% and 69% for *n-*, *sec*- and *tert*-butanol, respectively) [24–26]. Since the β-C–H bond energies in the molecular structures of different butanol isomers are very close (around 100 kcal/mol [3]), the number of β-C–H bonds (*iso*-butanol < *n*-butanol < *sec*-butanol < *tert*-butanol) determines the efficiency of this reaction class. The modeling results of different butanol isomers confirm a good linear relationship between the number of β-C–H bonds and the contribution of water elimination reaction.

$$iC_4H_9OH => iC_3H_7 + CH_2OH \quad (R1)$$

$$iC_4H_9OH = iC_4H_8 + H_2O \quad (R2)$$

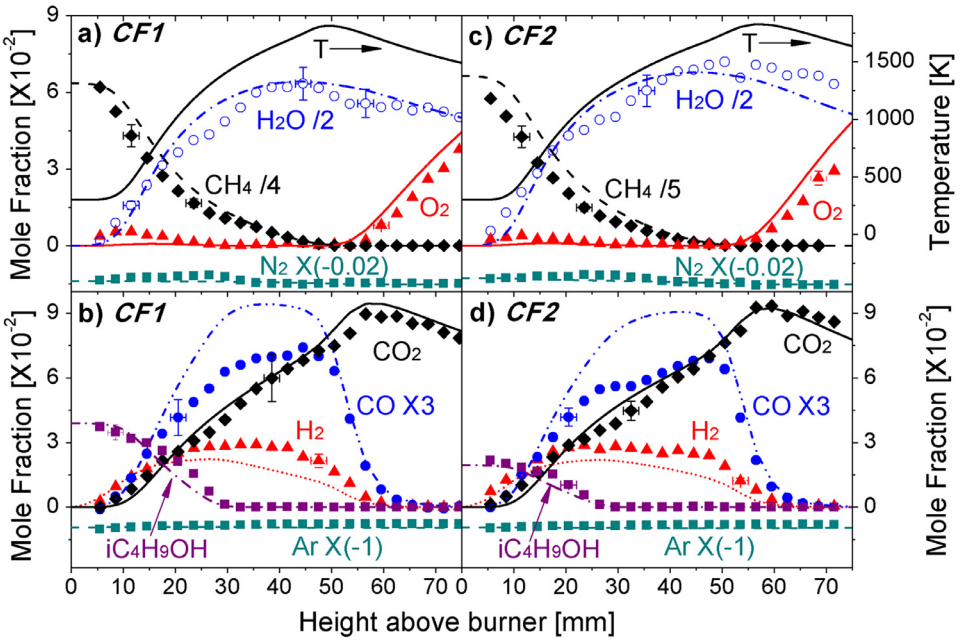

Fig. 1. Model prediction (lines) and experimental data (symbols) of major flame species in coflow diffusion flames, CF1 (a, b) and CF2 (c, d). The scale of the simulated temperature profiles in (a) and (c) is given on the right axis.

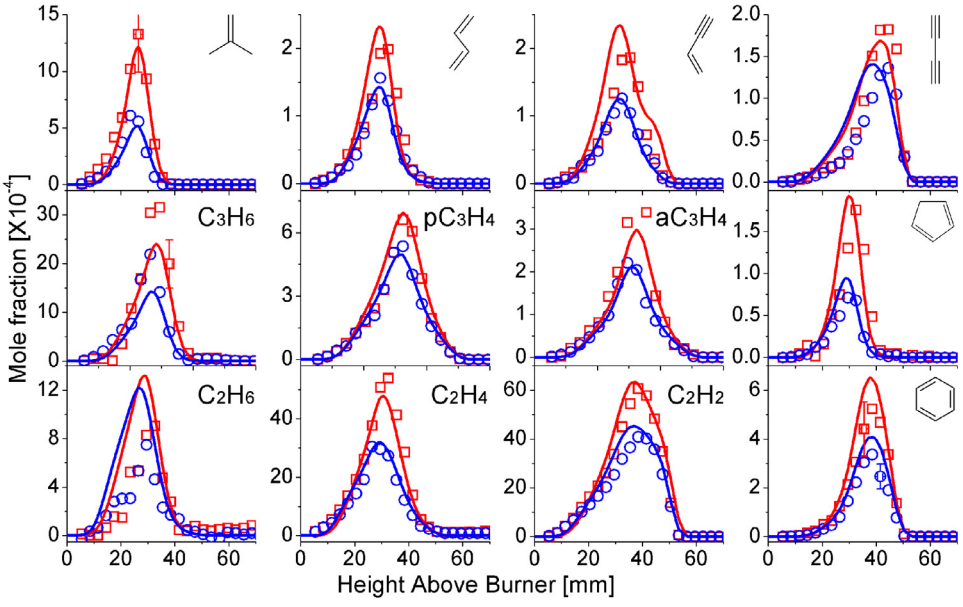

Fig. 2. Model predictions (solid lines) and experimental data (symbols) of the small hydrocarbon intermediates, cyclopentadiene and benzene. Red square and blue circle represent CF1 and CF2. (For interpretation of the references to color in this figure legend, the reader is referred to the web version of this article.)

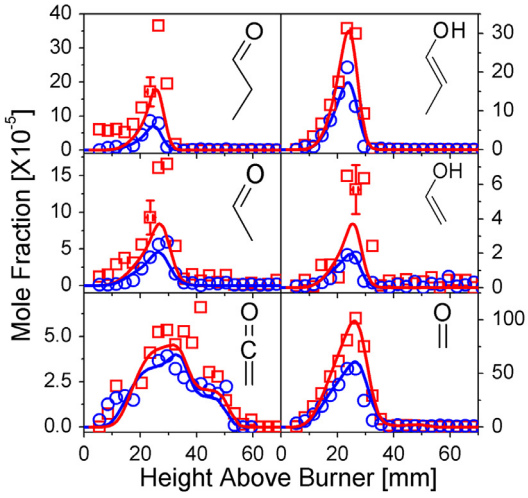

Fig. 3. Model predictions (solid lines) and experimental data (symbols) of the oxygenated intermediates. Red square and blue circle represent CF1 and CF2. (For interpretation of the references to color in this figure legend, the reader is referred to the web version of this article.)

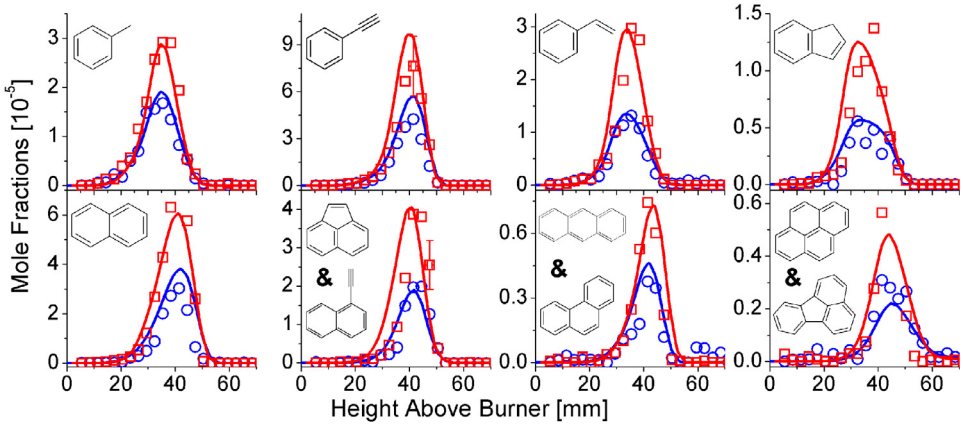

Fig. 4. Model predictions (solid lines) and experimental data (symbols) of the aromatic species. Red square and blue circle represent CF1 and CF2. (For interpretation of the references to color in this figure legend, the reader is referred to the web version of this article.)

$$i\mathrm{C_4H_9OH} = \mathrm{CH_3CH^*CH_2OH} + \mathrm{CH_3} \qquad \text{(R3)}$$

H abstraction reactions of *iso*-butanol mainly produce three $i\mathrm{C_4H_8OH}$ radicals, among which, the most favorable radical is $\alpha\mathrm{C_4H_8OH}$. Its decomposition dominantly forms propenol ($\mathrm{CH_3CHCHOH}$), while *iso*-butanal ($(\mathrm{CH_3})_2\mathrm{CHCHO}$) is its minor product. Then, propenol could form propanal via the enol-aldehyde tautomerization reaction, which will decompose to ethylene and formaldehyde. $\beta\mathrm{C_4H_8OH}$ consumes 18% of the *iso*-butanol, and converts to *iso*-butene ($i\mathrm{C_4H_8}$). The formed $i\mathrm{C_4H_8}$ mainly decomposes to $i\mathrm{C_4H_7}$ radial, which will yield allene by β-C–C scission reaction. $\gamma\mathrm{C_4H_8OH}$ consumes of 10% of *iso*-butanol, and converts to propene.

Propene is a key intermediate in the decomposition of *iso*-butanol. Its most efficient pathway is the decomposition of $i\mathrm{C_3H_7}$ radical, and the secondary one is the decomposition of $\mathrm{CH_3CH^*CH_2OH}$ radical. Both $i\mathrm{C_3H_7}$ and $\mathrm{CH_3CH^*CH_2OH}$ radicals are derived from the unimolecular decomposition of *iso*-butanol (R1) and (R2). For the decomposition of propene, there are two major pathways, 55% for allyl radical and 26% for ethylene. Allyl radical will then form allene and subsequently propargyl radical, which is an important precursor for PAHs. In general, propargyl radical can be formed through the decomposition of *iso*-butanol

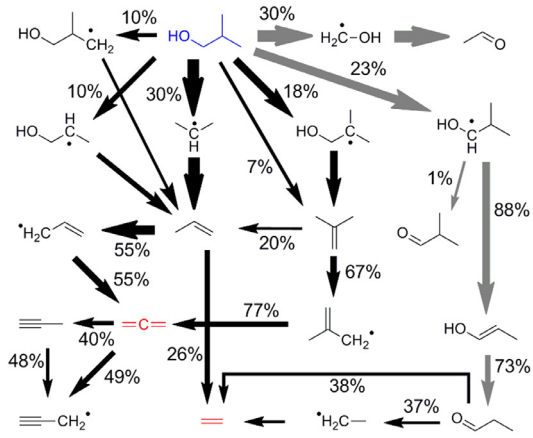

Fig. 5. Main decomposition pathways of iso-butanol in CF1. The thickness of the arrow is proportional to the carbon flux of the pathway. And the conversion of each step is labeled beside the arrow. The pathways forming oxygenated species are highlighted with gray arrows.

in two approximately contributed pathways: $iC_4H_9OH \rightarrow iC_3H_7 \rightarrow C_3H_6 \rightarrow aC_3H_5 \rightarrow aC_3H_4 \rightarrow C_3H_3$ and $iC_4H_9OH \rightarrow \beta C_4H_8OH \rightarrow iC_4H_8 \rightarrow iC_4H_7 \rightarrow aC_3H_4 \rightarrow C_3H_3$.

Since it is also a methane flame, propargyl radical can be also formed via a series of reactions from methyl radical [23]. The self-combination of methyl radical forms ethane and ethyl radical. Their subsequent decomposition sequences will lead to the formation of acetylene. And the reaction between methyl radical and acetylene is the major propyne formation pathway [25,26,41], which will decompose to propargyl radical. But ROP analysis shows a much less efficiency compared to the direct formation from iso-butanol.

4.2. Formation of aromatics

Benzene is formed mainly via the self-combination of propargyl radical. Phenyl radical that formed via the H abstraction of benzene and the combination of propargyl and propargylene radical (CH^*CCH^*) is very active in the growth of aromatics. Monocyclic aromatics, such as toluene, styrene, and phenylacetylene can be formed via the addition of methyl, ethylene and acetylene on phenyl radical. The decomposition of toluene yields benzyl radical, while the combination of methyl and phenyl has almost identical contribution for benzyl formation. The reaction of cyclopentadienyl and propargyl radicals (R4) is very efficient in the formation of styrene due to the addition of *iso*-butanol. As shown in Fig. 5, large amount of allyl radical is formed, which benefits the formation of cyclopentadiene via its reaction with acetylene. Cyclopentadienyl is the decomposition product of cyclopentadiene. ROP analysis reveals a contribution of 38% from R4, which is even higher than the combination of phenyl and ethylene. This pathway is not efficient in methane coflow flame [23], however, it was found important in the methane flames doped with butanol isomers [24–26], especially *iso*-butanol.

$$C_5H_5 + C_3H_3 = C_6H_5C_2H_3 + H \quad \text{(R4)}$$

Bicyclic to tetracyclic polycyclic aromatic hydrocarbons (PAHs) were observed in this work, such as indene, naphthalene, acenaphthylene/ethynylnaphthalene ($C_{12}H_8$), phenanthrene/anthracene ($C_{14}H_{10}$), and pyrene/fluoranthene ($C_{16}H_{10}$). Indene is formed via the reactions of benzene, phenyl and benzyl radical with C_2–C_3 species. Among them, the addition of propyne, allene and propargyl radical on phenyl radical and the combination of benzyl radical with acetylene provide contributions of 25% and 36% in CF1, respectively. The contribution from the combination of propargyl and benzene (15%) is relatively high due to the small amount of active free radical in the center of coflow flames [23–26]. Benzyl, phenyl, cyclopentadienyl radical, and phenylacetylene are precursors of naphthalene. Among them, the benzyl pathway is dominant. Benzyl radical can also undergo another pathway to form naphthalene via an intermediate radical of fulvenallyl (C_7H_5), as shown in Fig. 6. It is worthy to mention that the self-combination of cyclopentadienyl radical increases its contribution with the doping of *iso*-butanol [23], although it is still a minor pathway like the reaction of phenyl and vinylacetylene and the HACA channel of phenylacetylene. The combination of indenyl and propargyl radical is the dominant formation pathway of acenaphthylene, as emphasized in [33]. And phenanthrene is mainly formed through the combination of indenyl and cyclopentadienyl radicals. The precursors for the isomers of $C_{16}H_{10}$, including fluoranthene and

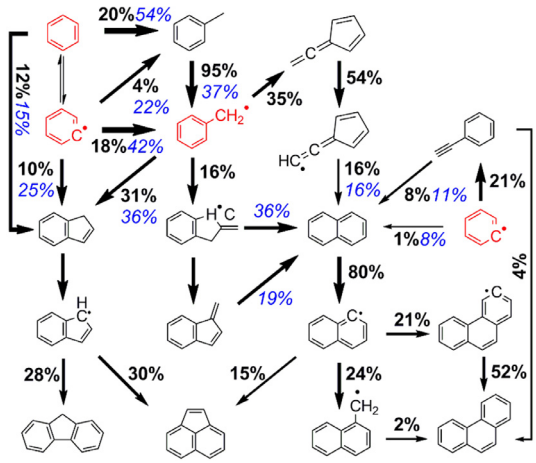

Fig. 6. Main aromatic formation pathways in CF1. The thickness of the arrow is proportional to the carbon flux of the pathway. Black bold and blue italic numbers aside the arrows indicate the ratios of the conversion and the formation for the specified species. (For interpretation of the references to color in this figure legend, the reader is referred to the web version of this article.)

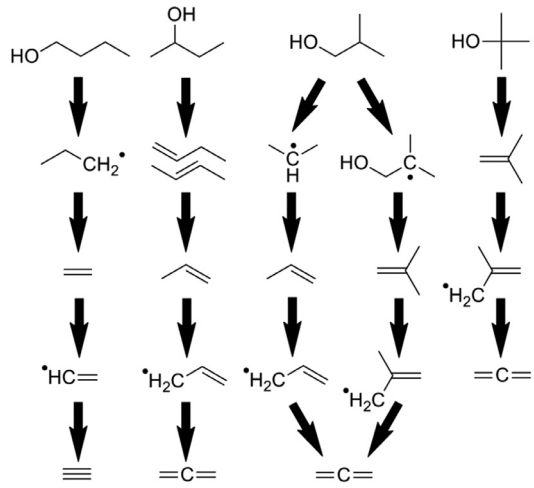

Fig. 7. Major formation pathways of propargyl radical in methane coflow flames doped with different butanol isomers [24–26].

pyrene, are naphthyl and acenaphthylene in this model.

4.3. *Fuel structure influence in aromatics formation of butanol isomers*

According to the analysis in Section 4.2 and the former studies on methane coflow flames doped with other butanol isomers [24–26], the major PAH formation pathways are the resonantly stabilized free radical involved reactions. Propargyl radical is the key species among these procedures. The sooting tendency of such kind of flame is usually determined by its formation efficiency in the decomposition of the doped butanol isomers. Figure 7 presents these pathways, and each arrow indicates an elementary reaction step. *n*-butanol does not obtain a direct pathway for the production of propargyl radical, thus needs the less efficient combination reaction of methyl and acetylene. It explains its lowest sooting tendency among the four isomers [10,11] and the similar sooting tendency to *n*-butane [10,20]. *Tert*-butanol has the most efficient and shortest pathway, therefore yields the highest quantity of PAHs in coflow flames and has the largest sooting tendency [10,11]. Both *sec*-butanol and *iso*-butanol undergo four intermediates for propargyl radical. *Sec*-butanol forms C_3

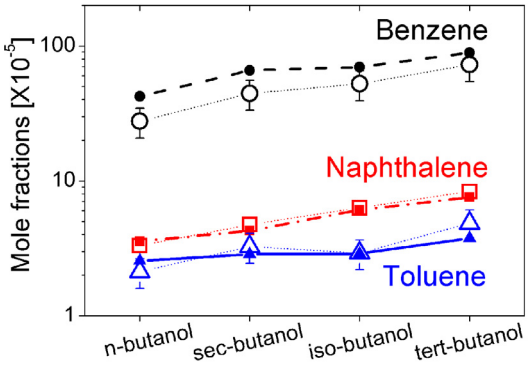

Fig. 8. Model predictions (lines with solid symbols) and experimental data (hollow symbols) of the maximum mole fractions of aromatics in methane coflow flames doped with different butanol isomers [24–26].

species via the further decomposition of 1- and 2-butene, while *iso*-butanol directly forms iC_3H_7 radical in its primary step and has an additional formation pathway of C_3 species via *iso*-butene. Therefore, the propargyl formation pathway in *sec*-butanol flame is less efficient. In summary, the index of this efficiency in butanol isomer flames is *tert*-butanol > *iso*-butanol > *sec*-butanol > *n*-butanol. Figure 8 compares the model predictions and experimental measurements of the maximum mole fractions of some typical aromatic species, like benzene, toluene and naphthalene, in methane coflow flames doped with different butanol isomers (3.8% of butanol isomer in the same gas inlet condition) [22– 24]. According to experimental measurements, the highest mole fractions of aromatics are from tert-butanol flame, while the lowest from *n*-butanol flame. The amounts of benzene and toluene are slightly higher in *iso*-butanol flame than *sec*-butanol flame, while the mole fraction of naphthalene is obviously higher in *iso*-butanol flame. The general trends of these typical aromatic species in experimental measurements agree well with those from the kinetic analysis. Therefore, it can be concluded that the sooting tendency of butanol isomers relates strictly to the efficiency of the propargyl formation pathways in fuel decomposition.

5. Conclusions

In this work, laminar coflow diffusion flames fueled with methane and *iso*-butanol were studied at atmospheric pressure. A kinetic model was developed from our previous *iso*-butanol and methane models to simulate the fuel decomposition process as well as the PAHs formation in the experiment. Compared to the coflow flames doped with other butanol isomers with the identical condition, the water elimination reaction of *iso*-butanol has the lowest contribution to its consumption. Two reaction pathways provide major contribution to the formation of propargyl radical, i.e. $iC_4H_9OH \rightarrow iC_3H_7 \rightarrow C_3H_6 \rightarrow aC_3H_5 \rightarrow aC_3H_4 \rightarrow C_3H_3$ and $iC_4H_9OH \rightarrow \beta C_4H_8OH \rightarrow iC_4H_8 \rightarrow iC_4H_7 \rightarrow aC_3H_4 \rightarrow C_3H_3$, which in turn determine the amounts of PAHs produced in *iso*-butanol flames. The amount of PAHs increases significantly with the increment of the doping ratio of *iso*-butanol. Propargyl is concluded as the key precursor for aromatics, while phenyl and benzyl radicals are the main PAH precursors. Finally, based on the studies of laminar coflow flames fueled with butanol isomers, the sooting tendency of butanol isomers relates strictly to the efficiency of the propargyl formation pathways in fuel decomposition.

Acknowledgments

Authors are grateful for funding supports from Natural Science Foundation of China (51476155, U1332208), National Basic Research Program of China (973 Program) (2013CB834602), Anhui Provincial Natural Science Foundation (1408085J09), Chinese Universities Scientific Fund (WK2320-000020) and Chinese Academy of Sciences.

Supplementary materials

Supplementary material associated with this article can be found, in the online version, at doi: 10.1016/j.proci.2016.06.111.

References

[1] P.P. Lin, K.S. Rabe, J.L. Takasumi, M. Kadisch, F.H. Arnold, J.C. Liao, *Metab. Eng.* 24 (2014) 1–8.
[2] S.M. Sarathy, P. Oßwald, N. Hansen, K. Kohse-Höinghaus, *Prog. Energy Combust. Sci.* 44 (2014) 40–102.

[3] K. Yasunaga, T. Mikajiri, S.M. Sarathy, et al., *Combust. Flame* 159 (2012) 2009–2027.
[4] J. Cai, W. Yuan, L. Ye, et al., *Combust. Flame* 161 (2014) 1955–1971.
[5] I. Stranic, S.H. Pyun, D.F. Davidson, R.K. Hanson, *Combust. Flame* 160 (2013) 1012–1019.
[6] C. Togbé, A. Mze-Ahmed, P. Dagaut, *Energy Fuels* 24 (2010) 5244–5256.
[7] B. Yang, P. Osswald, Y.Y. Li, et al., *Combust. Flame* 148 (2007) 198–209.
[8] P. Oßwald, H. Guldenberg, K. Kohse-Hoinghaus, B. Yang, T. Yuan, F. Qi, *Combust. Flame* 158 (2011) 2–15.
[9] N. Hansen, S.S. Merchant, M.R. Harper, W.H. Green, *Combust. Flame* 160 (2013) 2343–2351.
[10] C.S. McEnally, L.D. Pfefferle, *Proc. Combust. Inst.* 30 (2005) 1363–1370.
[11] H.F. Jin, Y.Z. Wang, K.W. Zhang, H.S. Guo, F. Qi, *Proc. Combust. Inst.* 34 (2013) 779–786.
[12] F. Wu, C.K. Law, *Combust. Flame* 160 (2013) 2744–2756.
[13] P.S. Veloo, F.N. Egolfopoulos, *Proc. Combust. Inst.* 33 (2010) 987–993.
[14] W. Liu, A.P. Kelley, C.K. Law, *Proc. Combust. Inst.* 33 (2011) 995–1002.
[15] T. Knorsch, A. Zackel, D. Mamaikin, L. Zigan, M. Wensing, *Energy Fuels* 28 (2014) 1446–1452.
[16] I. Stranic, D.P. Chase, J.T. Harmon, S. Yang, D.F. Davidson, R.K. Hanson, *Combust. Flame* 159 (2012) 516–527.
[17] J.T. Moss, A.M. Berkowitz, M.A. Oehlschlaeger, et al., *J. Phys. Chem. A* 112 (2008) 10843–10855.
[18] R. Grana, A. Frassoldati, T. Faravelli, et al., *Combust. Flame* 157 (2010) 2137–2154.
[19] S.M. Sarathy, S. Vranckx, K. Yasunaga, et al., *Combust. Flame* 159 (2012) 2028–2055.
[20] C.S. McEnally, L.D. Pfefferle, *Environ. Sci. Technol.* 45 (2011) 2498–2503.
[21] G. Karavalakis, D. Short, D. Vu, M. Villela, A. Asa-Awuku, T.D. Durbin, *Fuel* 128 (2014) 410–421.
[22] A. Elfasakhany, *Energy Convers. Manag.* 95 (2015) 398–405.
[23] H.F. Jin, A. Frassoldati, Y.Z. Wang, et al., *Combust. Flame* 162 (2015) 1692–1711.
[24] H.F. Jin, J.H. Cai, G.Q. Wang, et al., *Combust. Flame* 169 (2016) 154–170.
[25] H.F. Jin, W.H. Yuan, Y.Z. Wang, et al., *Proc. Combust. Inst.* 35 (2015) 863–871.
[26] H.F. Jin, A. Cuoci, A. Frassoldati, et al., *Combust. Flame* 161 (2014) 657–670.
[27] Photonionization Cross Section Database (Version 1.0), National Synchrotron Radiation Laboratory, Hefei, China, 2011, available at http://www.flame.nsrl.ustc.edu.cn/en/database.htm.
[28] C.W. Zhou, S.J. Klippenstein, J.M. Simmie, H.J. Curran, *Proc. Combust. Inst.* 34 (2013) 501–509.
[29] J. Zheng, R. Meana-Pañeda, D.G. Truhlar, *J. Am. Chem. Soc.* 136 (2014) 5150–5160.
[30] G.A. Pang, R.K. Hanson, D.M. Golden, C.T. Bowman, *J. Phys. Chem. A* 116 (2012) 4720–4725.
[31] W. Yuan, Y. Li, P. Dagaut, J. Yang, F. Qi, *Combust. Flame* 162 (2015) 22–40.
[32] G. Blanquart, P. Pepiot-Desjardins, H. Pitsch, *Combust. Flame* 156 (2009) 588–607.
[33] N.A. Slavinskaya, U. Riedel, S.B. Dworkin, M.J. Thomson, *Combust. Flame* 159 (2012) 979–995.
[34] H. Wang, M. Frenklach, *Combust. Flame* 110 (1997) 173–221.
[35] E. Goos, A. Burcat, B. Ruscic, Ideal Gas Thermochemical Database with Updates from Active Thermochemical Table, 2005, http://garfield.chem.elte.hu/Burcat/burcat.html.
[36] R.J. Kee, J. Warnatz, J.A. Miller, *A Fortran Chemical Kinetics Package for the Evaluation of Gas-Phase Viscosities, Conductivities and Diffusion Coefficient*, Sandia National Laboratory, 1983.
[37] H. Wang, M. Frenklach, *Combust. Flame* 96 (1994) 163–170.
[38] A. Cuoci, A. Frassoldati, T. Faravelli, E. Ranzi, *Energy Fuels* 27 (2013) 7730–7753.
[39] S. Chapman, T.G. Cowling, *The Mathematical Theory of Non-Uniform Gases*, Cambrige University Press, Cambrige, 1970.
[40] R.J. Hall, J. Quant, *Spectrosc. Radiat. Transf.* 49 (1993) 517–523.
[41] A. Cuoci, A. Frassoldati, T. Faravelli, et al., *Proc. Combust. Inst.* 34 (2013) 1811–1818.